Letter

Additional jamming transition in two-dimensional bidisperse granular packings

Juan C. Petit [1] and Matthias Sperl [1,2]

[1] Institute of Materials Physics in Space, German Aerospace Center (DLR), 51170 Köln, Germany

[2] Institut für Theoretische Physik, Universität zu Köln, 50937 Köln, Germany

(Received 24 February 2025; accepted 16 May 2025; published 20 June 2025)

We present a jamming diagram for two-dimensional bidisperse granular systems, capturing two distinct jamming transitions. The first occurs as large particles form a jammed structure, while the second, emerging at a critical small-particle concentration, $X_S^* \approx 0.21$, and size ratio, $\delta^* \approx 0.25$, involves small particles jamming into the voids of the existing large-particle structure upon further compression. Below this threshold, small particles fill voids within the large-particle network, increasing packing density. Beyond this point, excess small particles disrupt efficient packing, resulting in looser structures. These results, consistent with previous three-dimensional studies, demonstrate that the second transition occurs at a well-defined point in the (X_S, δ) plane, independent of dimensionality, likely driven by the geometric saturation of available space around particles, void closure, and structural arrangement.

DOI: 10.1103/mtcv-dbpd

The jamming transition occurs when granular materials shift from a fluidlike state, where particles can move freely, to a solid-like state, where most particles become immobilized. This phenomenon arises at a critical density, ϕ_J, when increasing compression or particle packing density restricts their motion, effectively freezing the system into a jammed configuration. This transition has been extensively studied in both two- (2D) and three-dimensional (3D) monodisperse and bidisperse packings [1–15]. In monodisperse sphere packings, the jamming transition occurs at $\phi_J \approx 0.64$ [1,4,6,7]. In contrast, bidisperse packings exhibit a broader range of ϕ_J values, increasing with lower size ratios δ and lower concentrations of small particles X_S [8,11–13,15,16]. Studies reveal that, in asymmetric bidisperse packings, the system transitions from a small-sphere-rich to a small-sphere-poor structure. This transition is caused by an abrupt drop in the number of small particles contributing to the jammed structure at a specific X_S, leaving the remaining small particles without contacts [8,15]. Recent work [14] identified an additional jamming transition line in 3D bidisperse systems, arising from the jamming of small particles that were previously without contacts. An emerging point is observed at $X_S^*(\delta^*) \approx 0.21$ with $\delta^* \approx 0.22$, below which two distinct jamming transitions occur: one dominated by large particles at lower ϕ, followed by a second, discontinuous jamming of small particles at higher ϕ. This second transition not only exhibits unique mechanical properties, as demonstrated in Refs. [17,18], but also enriches the jamming diagram for 3D bidisperse packings.

While the behavior of 3D packings reveals intricate jamming phenomena, 2D monodisperse and bidisperse systems are widely used to simplify and deepen our understanding. In polycrystalline monodisperse disk packings, the jamming transition occurs around $\phi_J \approx 0.88$ [1,2], whereas in disordered configurations, it drops to approximately $\phi_J \sim 0.81$ [2,9,10]. In binary systems with a size ratio of $\delta = 0.71$ and equal particle concentration (50:50), jamming occurs at $\phi_J \approx 0.84$ [4,5]. Systematic studies of the jamming transition have revealed a complex jamming diagram across the range $\delta, X_S \in [0, 1]$ (see Ref. [9]), with a more detailed mapping provided in Ref. [3]. These works demonstrate a maximum ϕ_J at low δ and high X_S. Notably, Ref. [3] highlights that the maximum ϕ_J is accompanied by a high number of small particles acting as rattlers, trapped in gaps between large particles and contributing minimally to the jammed structure. This behavior points to a decoupling in the jamming process of small and large particles, suggesting the presence of an additional transition line within the packing. In this work, we explicitly demonstrate that a second jamming transition can be rigorously identified, similar to that observed in 3D bidisperse packings [14]. This additional transition line is identified for $X_S < X_S^*(\delta^*) \approx 0.21$ and $\delta < \delta^* \approx 0.25$, distinguishing a jammed structure formed solely by large particles at low ϕ from one that incorporates both small and large particles at higher ϕ. The transition diagram for this case is illustrated in Fig. 1 and is further discussed later.

The MercuryDPM software [19] is used to simulate 2D bidisperse packings and employs the discrete element method. Packings consist of $N = 5000$ particles, with a number of large, N_L, and small, N_S, particles and radius r_L and r_S, respectively. The size ratio $\delta = r_S/r_L$, concentration of small particles $X_S = N_S\delta^2/(N_L + N_S\delta^2)$, and the overall packing fraction ϕ characterize the bidispersity of the system. An isotropic deformation, similar to that in Ref. [14], is applied here using the Hertzian spring dashpot contact model under the assumption of zero friction. Each bidisperse packing, defined by parameters (δ, X_S), is generated and subsequently

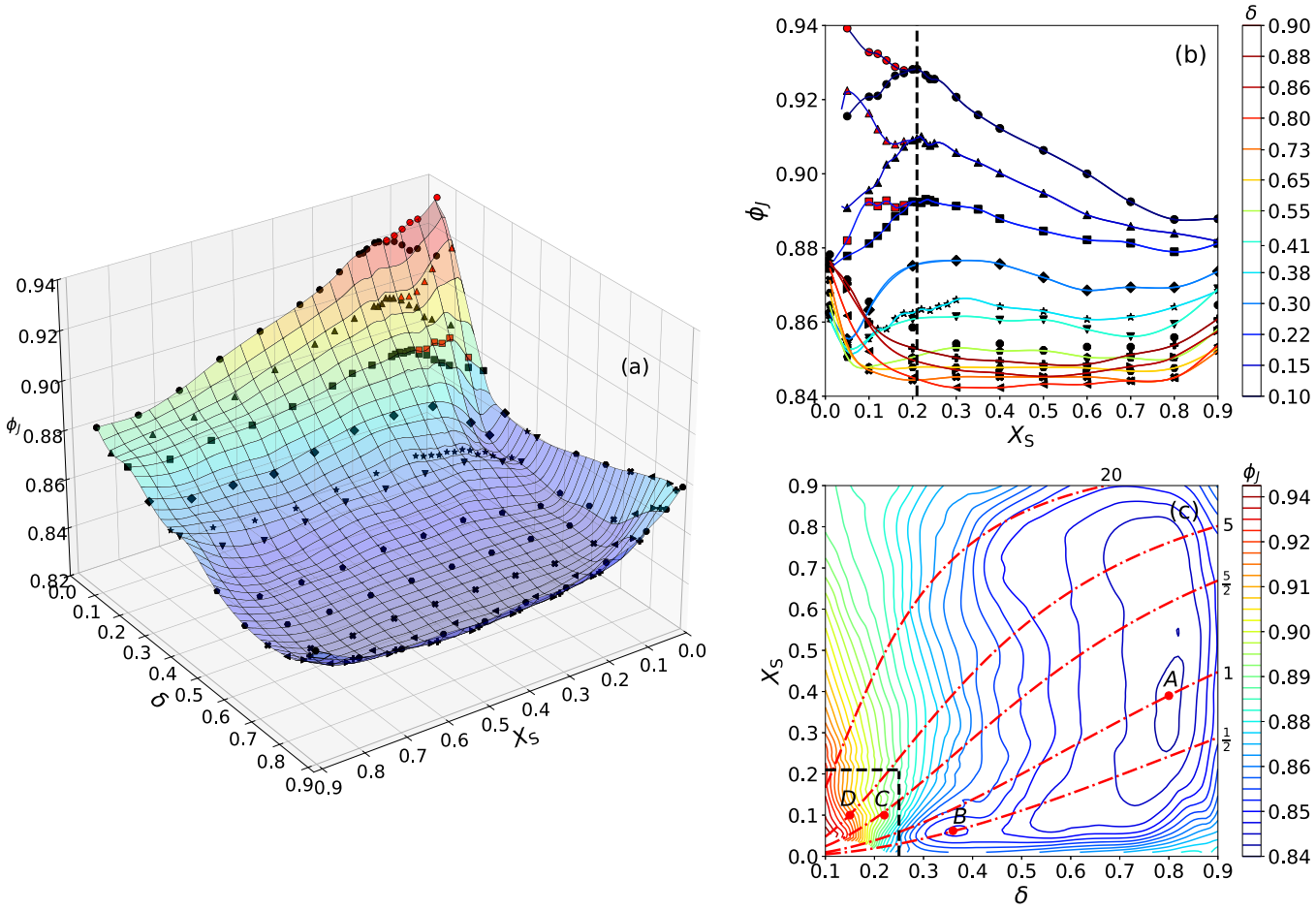

FIG. 1. Surface plot of the jamming density ϕ_J as a function of size ratio δ and small particle concentration X_S, with the color map representing ϕ_J. Black symbols (first transition) and red symbols (second transition) show simulation results averaged over three realizations, with standard deviations below 10^{-2} (not shown). These data points guide the surface fit and delineate the two jamming regimes. (b) Projection of ϕ_J-X_S for specific δ values from panel (a). (c) Contour plot of ϕ_J in the (δ, X_S) plane. Red dash-dotted lines show X_S-δ relations for various N_S/N_L ratios. Red dots (A–D) mark configurations in Fig. 3. Black dashed lines indicate the emerging point at $X_S^* \approx 0.21$ and $\delta^* \approx 0.25$, below which the second jamming transition occurs.

compressed and decompressed following a standardized protocol, as described in Sec. I of the Supplemental Material [20]. The jamming density, ϕ_J, at the first (second) transition is defined as the packing fraction at which a sudden increase is observed in the fraction of large (small) particles contributing to the jammed structure. These fractions are defined as $n_L(\phi) = N_L^c/N$ and $n_S(\phi) = N_S^c/N$, where $N_{L,S}^c$ represents the number of large and small particles in contact (see Sec. II of Ref. [20]). Figure 1(a) presents a surface jamming diagram (ϕ_J, δ, X_S), constructed via cubic interpolation of the measured ϕ_J values. The surface shows minima in ϕ_J at intermediate δ and a strong enhancement at low δ and X_S, with the color map emphasizing these variations. Different colored symbols represent simulation data and are overlaid to highlight the transitions: black symbols indicate the first jamming transition while red symbols denote the second. These transitions reflect distinct size-disparity effects, with further analysis given in Figs. 1(b)–1(c).

Figure 1(b) presents the projected ϕ_J-X_S relationship (solid lines) with corresponding simulation results (colored symbols) from Fig. 1(a). For $\delta \geqslant 0.65$, ϕ_J shows a slightly flat behavior for $X_S \in [0.1, 0.8]$ and a sudden increase at extreme values. For $\delta < 0.65$, ϕ_J increases exhibiting a maximum value at specific X_S, becoming prominent for lower δ. For $\delta \leqslant 0.22$, two distinct jamming transitions emerge from a common critical composition at $X_S^* \approx 0.21$, which we define as the emerging point. This bifurcation marks the onset of fundamentally different jamming regimes, separating regions where the system exhibits either a single ($X_S > X_S^*$) or two ($X_S < X_S^*$) jamming transitions. Typically, at low ϕ, the large particles jam first, defining the first jamming transition line (black symbols), while most small particles remain unjammed and do not yet contribute to the jammed structure. Upon further compression, the small particles become incorporated into the jammed network, leading to a second jamming transition (red symbols). This two-step process is most pronounced at low δ and low X_S, as illustrated in Figs. 1(a)–1(b). The shape of this second line depends on δ. For $\delta = 0.22$, a plateau in ϕ_J is observed. This plateau arises because small particles cannot fit into a triangular lattice of large particles after compression [see Fig. 3(c)], resulting in a constant ϕ_J over a range of X_S values. The decrease in ϕ_J at lower X_S indicates that the small particle count is insufficient to significantly enhance the overall density. For $\delta = 0.15$, small particles can now fit

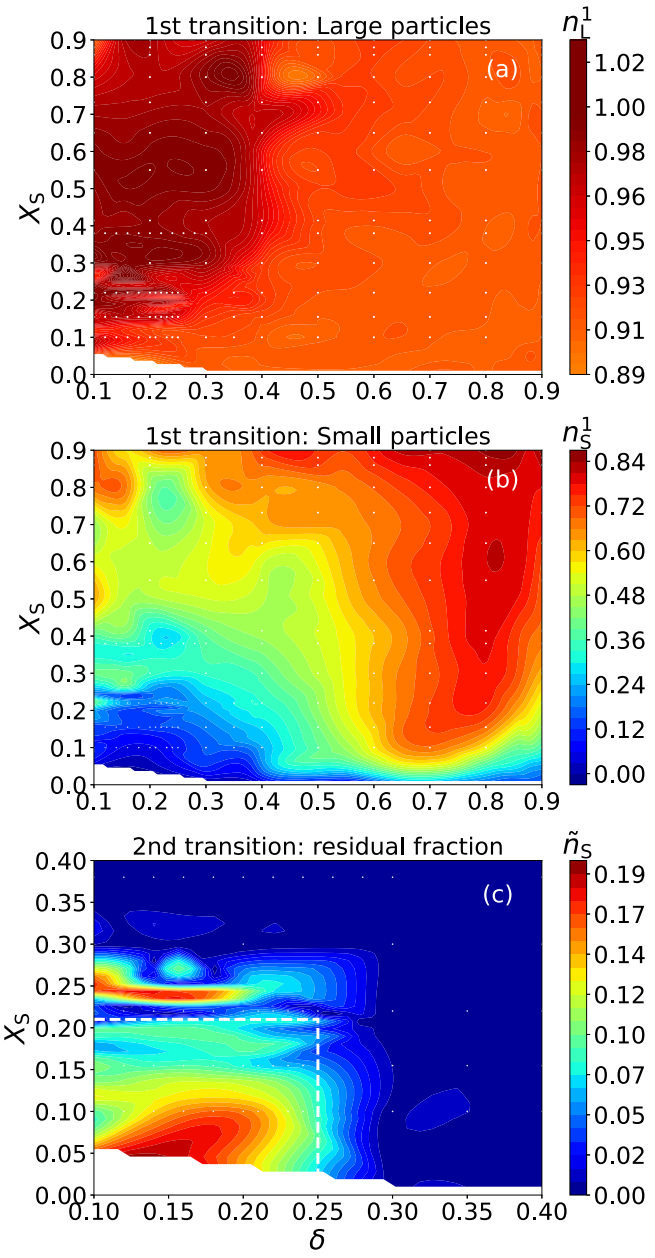

FIG. 2. Contribution of the nonrattler particle fraction ($Z \geqslant 4$) to the jamming transitions as a function of δ and X_S. (a) and (b) fraction of large, n_L^1, and small particles, n_S^1, at the first jamming transition. (c) Residual fraction of small particles, $\tilde{n}_S = n_S^2 - n_S^1$, at the second transition. n_S^2 at the second transition is included in the Supplemental Material [20]. The emerging point is found at $X_S^*(\delta^*) \approx 0.21$ and $\delta^* \approx 0.25$ (see white dashed lines).

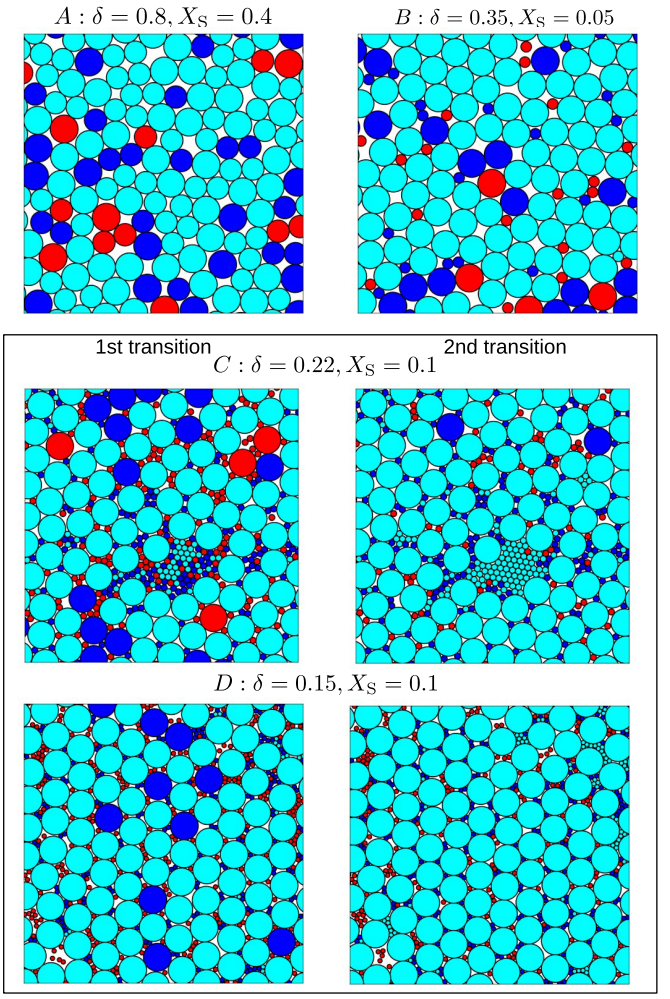

FIG. 3. Particle configurations at the first and second jamming transitions for various binary packings shown in Fig. 1(c). Cyan, blue, and red disks indicate particles with $Z \geqslant 4$, $Z = 3$, and $Z < 3$, respectively, marking rigid, marginally stable, and rattler particles. Color changes at the second transition reveal how large and small particles contribute to the evolving jammed backbone. These configurations offer a close-up view of representative regions within the overall system.

into the triangular lattice of large particles [see Fig. 3(d)], leading to an enhancement in ϕ_J (see Refs. [13,18]). A distinct scenario emerges for $\delta = 0.1$, where the small particles are so small that a substantial number are needed to fill the voids within the triangular lattice formed by the large particles. The overcompression required to jam the small particles alongside the large ones, resulting in the second transition, leads to a noticeable increase in the average particle overlap compared with the first jamming transition. This behavior is detailed in Sec. III of Ref. [20], where the average overlap along the second transition is shown to remain below 1% of the large particle diameter, decaying nearly to zero at the first transition. These overlap values provide strong evidence supporting the validity of the second jamming transition even after further compression.

Although the second jamming transition in 2D stems from the same physical mechanism as in 3D—jamming of small particles under continued compression—the Furnas model fails to capture either transition in 2D. While it successfully reproduces both transitions in 3D systems [14,17], it breaks down in 2D, as shown in Sec. IV of Ref. [20]. This is due to geometric constraints: in 3D, smaller particles can hierarchically fill volumetric voids (e.g., tetrahedral or octahedral), making the model's assumptions viable. In 2D, the flat voids between disks are too constrained to fit smaller particles without disrupting the packing, causing the model to overestimate density and miss the transitions. This challenges the Furnas

model's universality and calls for frameworks that explicitly account for dimensionality and structural heterogeneity.

The first and second jamming transition lines are identified by analyzing the fractions of small, n_S^X, and large, n_L^X, particles participating in the jammed structure, where the superscript $X \in \{1, 2\}$ denotes the corresponding jamming stage. Particles are considered part of the globally jammed backbone if they satisfy the criterion $Z \geqslant 4$, consistent with the isostatic condition for mechanical stability in 2D frictionless packings. Although $Z \geqslant 3$ ensures local stability [21], the stricter $Z \geqslant 4$ threshold isolates the subset of particles that actively sustain the global jammed network and define the structural backbone of the jammed state. Figure 2 shows n_S and n_L at the respective jamming transitions in the full range of δ and X_S values. For $\delta \geqslant 0.6$, where the flat behavior of ϕ_J is observed for X_S in Fig. 1(b), $n_L^1 \geqslant 90\%$ and $n_S^1 \geqslant 70\%$, which means that most of the large and small particles form the jammed structure [see Figs. 2(a) and 2(b)]. For $0.4 < \delta < 0.6$, n_L^1 remains constant while n_S^1 drops below 60%. Despite this reduction, large and small particles still contribute simultaneously to the jammed structure. For $\delta \leqslant 0.4$ and $X_S \lesssim 0.25$, n_S^1 is low while n_L^1 remains high [see Figs. 2(a) and 2(b)]. This implies that only large particles contribute to the jammed structure, while most small particles remain out of contact. This behavior defines the first jamming transition. With further compression, the fraction of small particles exhibits a sudden jump at higher ϕ, and after a significant incorporation into the already jammed structure of large particles defines the second jamming transition [see Fig. 1(b) and also Figs. 2(c) and 2(f) in Ref. [20]].

The fraction of small particles at the second transition, n_S^2, is similar to Fig. 2(b) except for a subtle change at low δ and low X_S (see Sec. V in Ref. [20]). To highlight this region, we quantify the difference $\tilde{n}_S = n_S^2 - n_S^1$, which captures the change in the fraction of small particles between the first and second transitions. For instance, $\tilde{n}_S = 0$, signifies that the fraction of small particles remains unchanged at the second transition, confirming that they become jammed together with the large particles during the first transition. Figure 2(c) shows the values of $\tilde{n}_S$ at the second transition. It illustrates a substantial increase in the number of small particles with $Z \geqslant 4$ contributing to the already jammed structure at low X_S and low δ. More than 10% of small particles are jammed, responsible for the second jamming transition shown in Figs. 1(a) and 1(b). The emerging point of the second transition is identified at $X_S^*(\delta^*) \approx 0.21$ and $\delta^* \approx 0.25$ (see white dashed lines), as this marks the boundary where regions with a substantial number of small particles are surrounded by low values of $\tilde{n}_S$. The smaller red region around $X_S \approx 0.25$ [see Fig. 2(c)] might be considered packings experiencing the second transition as well; however, this is not the case, as both large and small particles jam simultaneously in this region. This is just a continuous increase in the small particle number near the emerging point.

Figure 1(a) offers further insight that deepens our understanding of the jamming diagram, complemented by Fig. 1(c), which shows contour lines of constant ϕ_J. Two minima are observed: (a) a global minimum at $\delta \approx 0.8$ and $X_S \approx 0.4$, and (b) a local minimum at $\delta \approx 0.35$ and $X_S \approx 0.05$, exhibiting a similar jamming density. Interestingly, the global minimum corresponds to a 50:50 particle mixture, as shown by the dash-dotted lines in Fig. 1(c), which represent distinct ratios of small to large particles (N_S/N_L). Figure 3(a) provides a close-up view of the jammed particle configuration (cyan) at the global minimum, highlighting locally stable large and small particles (blue) as well as rattlers (red). In contrast, the local minimum at $\delta \approx 0.35$ corresponds to a packing where the number of small particles is roughly half that of the large ones. The particle configuration in Fig. 3(b) reveals that a greater fraction of small particles remain disconnected from the jammed backbone. These minima correspond to loose packings characterized by the lowest jamming density in bidisperse granular systems.

A jamming diagram surface similar to Fig. 1(a) was previously reported in Ref. [3], identifying the same minima but at different X_S values. This discrepancy arises from differing definitions of small particle concentration: their work uses the small particle fraction, $f_n = N_S/(N_S + N_L)$, while we adopt the area fraction, X_S. These definitions are related via $X_S = f_n\delta^2/(1 - f_n + f_n\delta^2)$, allowing us to confirm consistency between our minima and theirs. A key distinction in our diagram is the presence of additional transition lines at low δ and X_S [see red symbols in Fig. 1(a) and 1(b), absent in Ref. [3]]. However, their study highlights an increase in small particle rattlers within the same δ and X_S range, indicating the potential for a second transition. Black dashed lines in Fig. 1(c) mark the emerging point at $(X_S^*, \delta^*) \approx (0.21, 0.25)$, which defines the boundary for the consistent occurrence of the second jamming transition. Representative packings at $\delta = 0.22$ (c) and $\delta = 0.15$ (d) for $X_S = 0.1$ demonstrate systems with approximately five and five-and-a-half times more small particles than large ones. At the second transition, $\delta = 0.22$ exhibits a higher ϕ_J compared with the first transition, due to the incorporation of rattler particles into the jammed structure upon compression [see Fig. 3(c)]. In contrast, $\delta = 0.15$ represents a special size ratio where a single small particle can perfectly fill the void within a triangular lattice of large particles, satisfying $r_S = [(2 - \sqrt{3})/\sqrt{3}]r_L$. This configuration results in a denser packing and is observed in Fig. 3(d), particularly at the second transition and occasionally at the first one. Note that the second transition can occur across a wide range of particle ratios N_S/N_L. For the commonly studied 50:50 mixture ($N_S/N_L = 1$), the onset of the second transition is observed at $X_S \leqslant 0.05$. Introducing particle ratios N_S/N_L alongside the jamming diagram offers a clearer understanding of how large and small particles contribute to the jammed structure of the mixture.

In conclusion, we constructed a detailed surface jamming diagram (ϕ_J, δ, X_S) that presents both the first and second jamming transitions. The first transition is dominated by large particles, with small particles not contributing, while the second transition occurs as small particles jam into the already jammed structure of large particles. This second transition arises for $\delta \leqslant 0.25$ and $X_S < 0.21$, a range where the size asymmetry is so pronounced that, beyond the typical configuration where a small particle fills the voids of a triangular arrangement of large particles, numerous small particles occupy interstitial spaces, leading to an increased jamming density with further compression. Outside this range, small particles do not fit into the void of large ones, leading to

a looser packing. The second transition line and the emerging point values $\delta^* \approx 0.25$ and $X_S^*(\delta^*) \approx 0.21$ align with 3D results obtained using the linear contact model [14]. This consistency indicates that the transition is independent of the contact model and might suggest that its emerging point is governed primarily by the packing geometry of the mixture, specifically by the saturation of local space, void closure, and the emergence of structural arrangement. While our focus here has been on the geometrical and structural aspects of the second jamming transition in two dimensions, a deeper understanding of its physical nature, particularly through critical scaling analysis, remains an important open question. Previous work in 3D systems [22] showed distinct scaling behavior of the coordination number across the two transitions, while pressure scaling appears similar. Extending such an analysis to 2D systems is a promising direction for future work.

The two-step jamming transitions observed in Figs. 1(a) and 1(b) resemble the emergence of multiple arrested states in thermal systems, such as those found in binary hard-sphere mixtures with varying composition [23]. While the glass-glass transition reported in monodisperse colloids with short-range attractions [24] is driven by changes in interaction potential rather than composition, it exemplifies how distinct dynamical arrest mechanisms can coexist within a single system. In our case, the jamming process proceeds via two distinct stages: one dominated by the mechanical arrest of large particles, and a second involving the percolation of small particles into the jammed structure of large ones. This sequential arrest mirrors, in a geometric (athermal) context, the concept of multiple glassy states governed by different physical constraints. These analogies underscore the broader relevance of composition- and interaction-driven arrest, potentially informing unifying theoretical frameworks for both glass and jamming transitions [25,26].

The second jamming transition marks a qualitative shift in the packing structure and mechanical response of bidisperse granular materials. While the first transition is governed by the excluded area of large particles, the second arises from the saturation of voids by small particles—driven by their own excluded area—signaling a reorganization in space-filling and the onset of mechanical stability. The second transition reveals that jamming in mixtures of differently sized particles does not occur through a single, unified process. Instead, it can involve multiple, distinct transitions, each associated with a specific particle size and contributing uniquely to the emergence of rigidity through excluded area effects and spatial organization.

We thank T. Kranz and Th. Voigtmann for proofreading, fruitful discussions, and providing constructive criticism about the results and the paper. This work was supported by the German Academic Exchange Service (Deutscher Akademischer Austauschdienst) under Grant No. 57424730.

The data supporting this study's findings are available within the article.

[1] A. Donev, S. Torquato, F. H. Stillinger, and R. Connelly, Jamming in hard sphere and disk packings, J. Appl. Phys. **95**, 989 (2004).

[2] S. Meyer, C. Song, Y. Jin, K. Wang, and H. A. Makse, Jamming in two-dimensional packings, Physica A **389**, 5137 (2010).

[3] D. Koeze, D. Vågberg, B. Tjoa, and B. Tighe, Mapping the jamming transition of bidisperse mixtures, Europhys. Lett. **113**, 54001 (2016).

[4] C. S. O'Hern, L. E. Silbert, A. J. Liu, and S. R. Nagel, Jamming at zero temperature and zero applied stress: The epitome of disorder, Phys. Rev. E **68**, 011306 (2003).

[5] T. S. Majmudar, M. Sperl, S. Luding, and R. P. Behringer, Jamming transition in granular systems Phys. Rev. Lett. **98**, 058001 (2007).

[6] M. van Hecke, Jamming of soft particles: Geometry, mechanics, scaling and isostaticity, J. Phys.: Condens. Matter **22**, 033101 (2010).

[7] R. P. Behringer and B. Chakraborty, The physics of jamming for granular materials: A review, Rep. Prog. Phys. **82**, 012601 (2019).

[8] I. Prasad, C. Santangelo, and G. Grason, Subjamming transition in binary sphere mixtures, Phys. Rev. E **96**, 052905 (2017).

[9] T. Odagaki and A. Hoshiko, Random jammed packing of binary hard disks, J. Phys. Soc. Jpn. **71**, 2350 (2002).

[10] S. Atkinson, F. H. Stillinger, and S. Torquato, Existence of isostatic, maximally random jammed monodisperse hard-disk packings, Proc. Natl. Acad. Sci. USA **111**, 18436 (2014).

[11] I. Biazzo, F. Caltagirone, G. Parisi, and F. Zamponi, Theory of amorphous packings of binary mixtures of Hard spheres, Phys. Rev. Lett. **102**, 195701 (2009).

[12] A. B. Hopkins, Y. Jiao, F. H. Stillinger, and S. Torquato, Phase diagram and structural diversity of the densest binary sphere packings, Phys. Rev. Lett. **107**, 125501 (2011).

[13] N. Kumar, V. Magnanimo, M. Ramaioli, and S. Luding, Tuning the bulk properties of bidisperse granular mixtures by small amount of fines, Powder Technol. **293**, 94 (2016).

[14] J. C. Petit, N. Kumar, S. Luding, and M. Sperl, Additional transition line in jammed asymmetric bidisperse granular packings, Phys. Rev. Lett. **125**, 215501 (2020).

[15] Y. Hara, H. Mizuno, and A. Ikeda, Phase transition in the binary mixture of jammed particles with large size dispersity, Phys. Rev. Res. **3**, 023091 (2021).

[16] C. Furnas, Grading aggregates - I. - Mathematical relations for beds of broken solids of maximum density, Ind. Eng. Chem. **23**, 1052 (1931).

[17] J. C. Petit, N. Kumar, S. Luding, and M. Sperl, Bulk modulus along jamming transition lines of bidisperse granular packings, Phys. Rev. E **106**, 054903 (2022).

[18] J. C. Petit and M. Sperl, Structural transitions in jammed asymmetric bidisperse granular packings, Granul. Matter **25**, 43 (2023).

[19] T. Weinhart, L. Orefice, M. Post, M. P. van Schrojenstein Lantman, I. F. Denissen, D. R. Tunuguntla, J. Tsang, H. Cheng, M. Y. Shaheen, H. Shi, P. Rapino, E. Grannonio, N. Losacco, J. Barbosa, L. Jing, J. E. A. Naranjo, S. Roy, W. K. den Otter, and A. R. Thornton, Fast, flexible particle simulations—An

introduction to MercuryDPM, Comput. Phys. Commun. **249**, 107129 (2020).

[20] See Supplemental Material at http://link.aps.org/supplemental/10.1103/mtcv-dbpd for details of the simulation algorithms and definitions.

[21] L. E. Silbert, A. J. Liu, and S. R. Nagel, Structural signatures of the unjamming transition at zero temperature, Phys. Rev. E **73**, 041304 (2006).

[22] J. C. Petit and M. Sperl, Pressure model and scaling laws in jammed bidisperse granular packings, Granul. Matter **27**, 23 (2025).

[23] T. Voigtmann, Multiple glasses in asymmetric binary hard spheres, Europhys. Lett. **96**, 36006 (2011).

[24] M. Sperl, Dynamics in colloidal liquids near a crossing of glass- and gel-transition lines, Phys. Rev. E **69**, 011401 (2004).

[25] P. Charbonneau, J. Kurchan, G. Parisi, P. Urbani, and F. Zamponi, Glass and jamming transitions: From exact results to finite-dimensional descriptions, Annu. Rev. Condens. Matter Phys. **8**, 265 (2017).

[26] D. Hexner, A. J. Liu, and S. R. Nagel, Two diverging length scales in the structure of jammed packings, Phys. Rev. Lett. **121**, 115501 (2018).